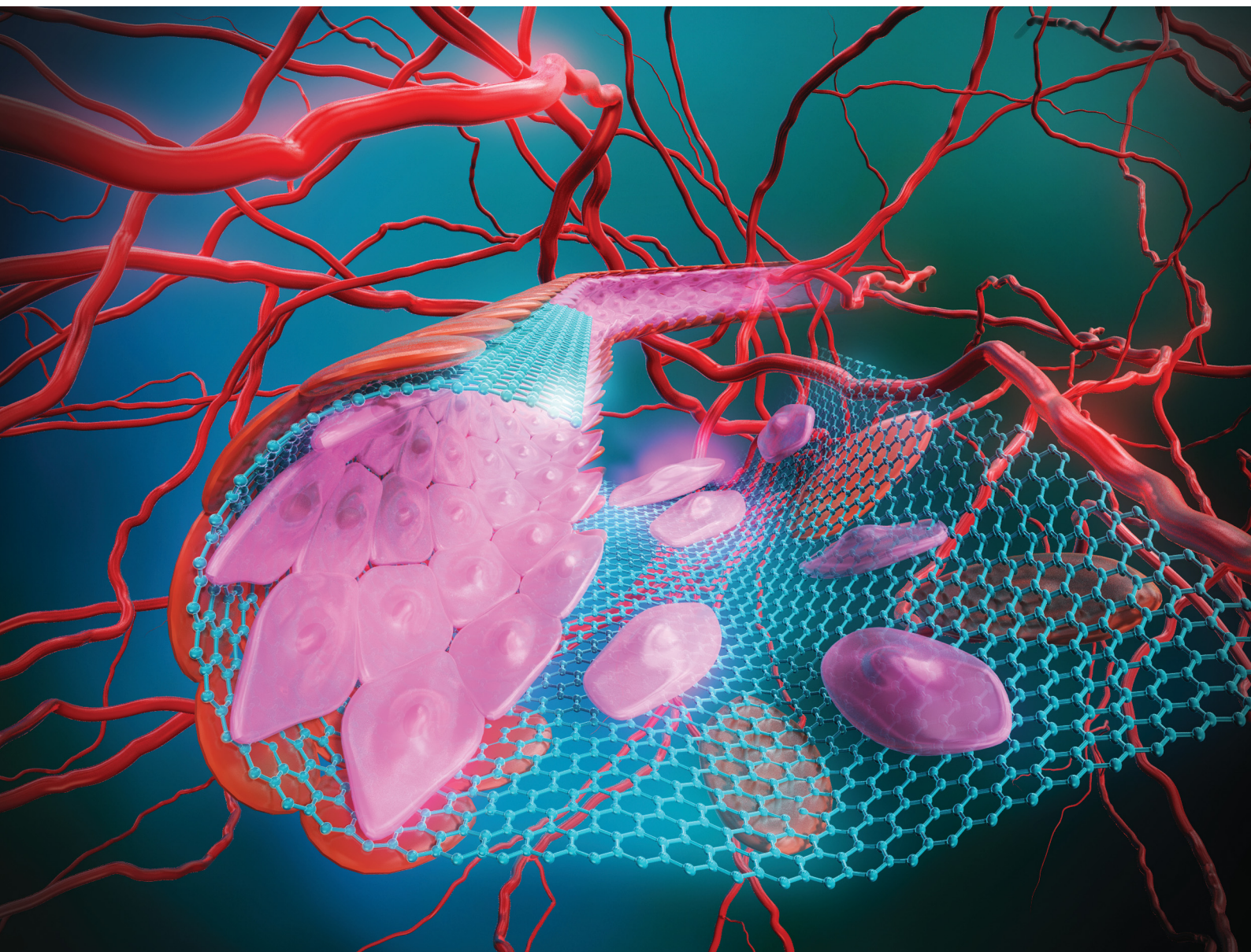


# Nanoscale Horizons

The home for rapid reports of exceptional significance in nanoscience and nanotechnology

[rsc.li/nanoscale-horizons](https://rsc.li/nanoscale-horizons)



ISSN 2055-6756







Cite this: *Nanoscale Horiz.*, 2023, 8, 1529

Received 20th July 2023,  
Accepted 21st September 2023

DOI: 10.1039/d3nh00304c

[rsc.li/nanoscale-horizons](https://rsc.li/nanoscale-horizons)

## Small-artery-mimicking multi-layered 3D co-culture in a self-folding porous graphene-based film†

Koji Sakai, \*<sup>a</sup> Shigenori Miura, <sup>b</sup> Tetsuhiko F. Teshima, <sup>c</sup> Toichiro Goto,<sup>a</sup> Shoji Takeuchi <sup>bde</sup> and Masumi Yamaguchi<sup>a</sup>

*In vitro* vessel-mimicking models have been spotlighted as a powerful tool for investigating cellular behaviours in vascular development and diseases. However, it is still challenging to create micro-scale tubular tissues while mimicking the structural features of small arteries. Here, we propose a 3D culture model of small vascular tissue using a self-folding graphene-based porous film. Vascular endothelial cells were encapsulated within the self-folding film to create a cellular construct with a controlled curvature radius ranging from 10 to 100  $\mu\text{m}$ , which is comparable to the size of a human arteriole. Additionally, vascular endothelial cells and smooth muscle cells were separately co-cultured on the inner and outer surfaces of the folded film, respectively. The porous wall worked as a permeable barrier between them, affecting the cell–cell communications like the extracellular layer in the artery wall. Thus, the culture model recapitulates the structural features of a small artery and will help us better understand intercellular communications at the artery wall in physiological and pathological conditions.

## Introduction

Vascular diseases in peripheral small arteries, including atherosclerosis and aneurysms, are the leading causes of severe

### New concepts

*In vitro* cell culture models mimicking blood vessel architectures have gained much attention due to their potential for biological applications. However, it remains challenging to reconstruct the cellular layer and ECM layer in small tubular tissue. In this study, we construct a ten-micron-scale tubular tissue in which endothelial cells and smooth muscle cells are laminated using a self-foldable graphene-based porous nanofilm. The porous nanofilm works as a cell scaffold as well as a permeable barrier between those cells, modulating the intercellular communications that are involved in various vascular pathogenesis. Our work, therefore, demonstrates the unique use of mechanical properties of carbon nanomaterials for tissue engineering and microphysiological systems, which will be of great interest to readers from many research fields, including biomedical engineering, nanomaterials engineering, and functional materials.

vascular diseases.<sup>1,2</sup> Despite the need to establish effective therapeutic strategies, vascular pathophysiology is still largely unclear due to the lack of adequate experimental models. Recently, vessel-mimicking *in vitro* models have gained much attention because they emulate the microenvironmental geometry, cellular composition, and extracellular matrix (ECM) structure, recapitulating the physiological and pathological cell behaviours under well-controlled experimental conditions.<sup>3,4</sup> Among them, the tubular structure is the most unique and ubiquitous architecture of blood vessels. Many tubular tissues have been created by various means, such as self-organized capillaries, microfluidics, moulding, and bioprinting.<sup>3–8</sup> However, forming micron-scale tubular tissue remains a technical challenge.

Self-folding materials and devices have been utilized as cell scaffolds with precise curved geometries.<sup>9–16</sup> A predetermined internal stress gradient inside a nanometre-thick film drives self-folding and forms a micro-scale cylindrical structure (micro-roll). By selecting biocompatible film materials, living vascular cells can be grown on the curved surface, and they form a cylindrical or tubular tissue.<sup>12–14</sup> For example, the outer surface of a ten-micron micro-roll was used as a scaffold for

<sup>a</sup> NTT Basic Research Laboratories and Bio-Medical Informatics Research Center, NTT Corporation, 3-1 Morinosato Wakamiya, Atsugi, Kanagawa, 243-0198, Japan. E-mail: [ko.sakai@ntt.com](mailto:ko.sakai@ntt.com)

<sup>b</sup> Institute of Industrial Science, The University of Tokyo, 4-6-1 Komaba, Meguro-ku, Tokyo 153-8505, Japan

<sup>c</sup> Medical and Health Informatics Laboratories, NTT Research Incorporated, 940 Stewart Dr, Sunnyvale, CA, 94085, USA

<sup>d</sup> Department of Mechano-Informatics, Graduate School of Information Science and Technology, The University of Tokyo, 7-3-1 Hongo, Bunkyo-ku, Tokyo 113-8656, Japan

<sup>e</sup> International Research Center for Neurointelligence (WPI-IRC/N), The University of Tokyo Institutes for Advanced Study (UTIAS), The University of Tokyo, 7-3-1 Hongo, Bunkyo-ku, Tokyo 113-0033, Japan

† Electronic supplementary information (ESI) available. See DOI: <https://doi.org/10.1039/d3nh00304c>

vascular endothelial cell culture to form a vascular-like tubular tissue.<sup>13</sup> Additionally, recent work developed a layer-by-layer co-culture of human vascular endothelial cells and smooth muscle cells on the inner wall of self-folding micro-rolls with a small diameter (50–300  $\mu\text{m}$ ).<sup>14</sup> Furthermore, in other methods to create tubular vascular constructs, co-culturing different cell types has been reported to be an effective way to investigate intercellular communications that have critical roles in vascular pathogenesis.<sup>4,5</sup> Therefore, further advances in co-culture methods using self-folding materials will make the small artery model more sophisticated.

To mimic the detailed structural characteristics of small arteries in the co-culture model, a layer of ECM should also be taken into consideration. In the wall of an artery, the internal elastic lamina (IEL) separates the endothelium and the smooth muscle. It forms a porous sheet affecting intercellular communications between them *via* the passage of diffusible substances, cell–cell contacts (myoendothelial junction), and cell migration, which are key events in vascular development and disease.<sup>17–19</sup> Since both the inner and outer walls of self-folding micro-rolls have been utilized as the cell culture surface,<sup>13,14</sup> it would be possible to co-culture two types of cells separately on each wall. Furthermore, incorporation of pores would enable us to control cell–cell interactions, like porous membranes in trans-well co-culture models and fluidic devices.<sup>20–22</sup> In fact, we have previously developed a graphene-based self-folding porous film and proved that micro-scale pores across the nanometre-thick film enable neurons inside the micro-roll to communicate with the surrounding neurons.<sup>15,16</sup> Both graphene and parylene-C, which were used as the inner and outer surfaces of the micro-roll, work as suitable cell scaffolds due to their excellent biocompatibility and transparency. Thus, the separated co-culture on the self-folding porous film will emulate the characteristics of small arteries, including micro-scale geometry, cellular composition, and ECM structure.

Here, we demonstrate the separated co-culture of vascular endothelial cells and smooth muscle cells on the self-folding porous micro-roll to create a cellular construct recapitulating key characteristics of small arteries. We encapsulate human umbilical vein endothelial cells (HUVECs) within the self-folding graphene-based film and create tubular tissue with a diameter ranging from 20 to 200  $\mu\text{m}$ , which is comparable to the human arteriole (15–300  $\mu\text{m}$ ).<sup>1,23</sup> Human umbilical artery smooth muscle cells (HUASMCs) are then seeded on the outer surface of the micro-roll. To confirm that HUVECs and HUASMCs are separately co-cultured, we observe how they grow on the inner and outer surfaces of the micro-roll and examine the spatial organization of cell layers by the three-dimensional (3D) reconstruction of confocal images.

## Experimental

### Fabrication process of the self-folding film

The self-folding film consists of a sacrificial Ca-alginate layer, graphene, and a parylene-C layer (Fig. 1A). As described in

previous studies,<sup>15,16,24</sup> the dissolution of the sacrificial Ca-alginate layer releases a bilayer of graphene and parylene-C, and an internal residual stress within the bilayer induces the bending. The composition of the bilayer is also maintained after self-folding, as confirmed by Raman spectroscopy.<sup>15,16,24</sup> Additionally, no clear defects were observed in the folded graphene. Thus, both materials can work as cell-scaffolds on the outer and inner surfaces of the micro-roll.

The self-folding film was fabricated as described in previous work.<sup>15,24,25</sup> The fabrication process is illustrated in Fig. S1 (ESI<sup>†</sup>). First, the Ca-alginate layer was formed on an 18  $\times$  18 mm glass substrate by the gelation of Na-alginate. To pattern the Ca-alginate layer, two 6  $\times$  18 mm masking tapes were attached to both outer sides of the substrate, and then a Na-alginate solution was spin-coated on the substrate. After the gelation of Na-alginate using a  $\text{CaCl}_2$  solution, the masking tape was removed, and then the 6  $\times$  18 mm Ca-alginate layer remained at the centre of the substrate. Next, chemical vapour deposition (CVD)-grown graphene monolayer (Graphene Platform) was released from Cu foil and transferred onto the Ca-alginate layer using the poly(methyl methacrylate) (PMMA)-assisted method. After removing the PMMA with acetone, the substrate was laminated with parylene-C using the CVD process (SCS, LABCOATER PSD2010). In this process, dichloro-di (*p*-xylylene) was vaporized at 175  $^\circ\text{C}$  and then pyrolyzed at 690  $^\circ\text{C}$  to generate a chloro-*p*-xylylene monomer. Chloro-*p*-xylylene was polymerized on the substrate surface with a vacuum pressure of 35 mTorr at room temperature. Finally, the multi-layered film was patterned by reactive ion etching with oxygen plasma through a photoresist mask (Rohm and Haas, S1813). Two cycles of etching with a power of 100 W and an  $\text{O}_2$  gas flow rate of 30 sccm for 6 min were conducted.

Representative patterns are illustrated in Fig. S2 (ESI<sup>†</sup>). The array of rectangular films with varied dimensions (width of 300–1000  $\mu\text{m}$ ; length of 1000–1500  $\mu\text{m}$ ) was supported by cross-shaped hinges. The hinges were connected to both outer sides of the substrate, which are never released due to the absence of a sacrificial layer. The dissolution of the sacrificial layer releases the rectangular films and induces the self-folding of the films while maintaining the position of the floated films by the supporting hinges. Consequently, the array of folded films can be stably positioned for microscopic observations even after medium exchanges. Additionally, 3  $\mu\text{m}$ -pores with pitches of 50  $\mu\text{m}$  were incorporated into rectangles to facilitate the diffusion of nutrients and oxygens inside the internal space of the folded film.

### Cell culture

Primary HUVECs, primary HUASMCs, and their culture media were purchased from PromoCell. HUVECs were cultured using Endothelial Cell Basal Medium 2 supplemented with 2% v/v fetal calf serum, 5  $\text{ng ml}^{-1}$  epidermal growth factor, 10  $\text{ng ml}^{-1}$  basic fibroblast growth factor, 20  $\text{ng ml}^{-1}$  insulin-like growth factor, 0.5  $\text{ng ml}^{-1}$  vascular endothelial growth factor 165, 1  $\mu\text{g ml}^{-1}$  ascorbic acid, 22.5  $\mu\text{g ml}^{-1}$  heparin, and 0.2  $\mu\text{g ml}^{-1}$  hydrocortisone. HUASMCs were cultured using Smooth Muscle Cell Basal Medium 2 supplemented with 5% v/v

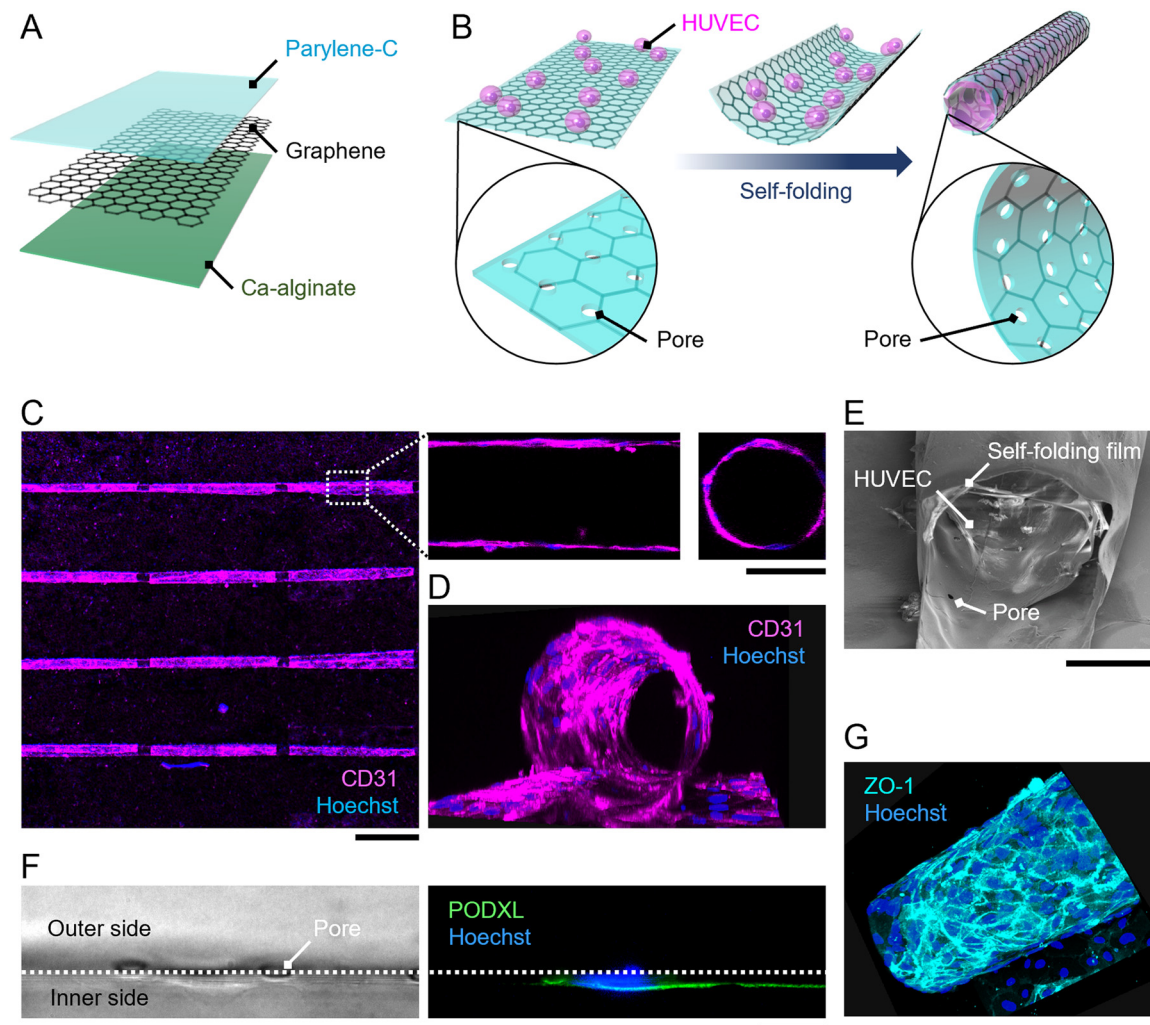


**Fig. 1** Three-dimensional HUVEC culture within a self-folded film. (A) Composition of the self-folding film. (B) Process of cell encapsulation within the self-folding film. Note that the pores across the film were retained even after self-folding. (C) Immunocytochemical images showing the array of cell-laden micro-rolls. In the magnified image, the top view and the cross-sectional view of a representative micro-roll indicate the tubular structure of the cellular construct. (D) 3D reconstruction of confocal immunocytochemical images showing the tubular tissue in the micro-roll. (E) Scanning electron microscopy image of a cell-laden micro-roll at the edge of the micro-roll. (F) Differential interference contrast and immunocytochemical images of the HUVECs attached to the inner surface of the micro-roll. It highly expressed PODXL at the apical side of the cell membrane. White dotted lines indicate the wall of the self-folding film. (G) 3D reconstruction of ZO-1 staining image showing the layer structure of HUVECs. ZO-1 was highly expressed at the cell boundary, indicating the formation of tight junctions. Scale bars indicate 500  $\mu\text{m}$  (C), 100  $\mu\text{m}$  (inset, C), and 20  $\mu\text{m}$  (F).

fetal calf serum, 0.5  $\text{ng ml}^{-1}$  epidermal growth factor, 2  $\text{ng ml}^{-1}$  basic fibroblast growth factor, and 5  $\text{ng ml}^{-1}$  insulin. For co-culture, those media were mixed in equal amounts. Cells with passage numbers 5 to 10 were detached from the cell culture dishes using 0.05% trypsin-EDTA to create a cell suspension.

For cell encapsulation, HUVECs were seeded on the self-folding film, and then the self-folding was induced by the dissolution of the sacrificial layer (Fig. 1B). Before seeding cells, the film was coated with fibronectin to enhance cell attachment and growth. To visualize the film under a fluorescent microscope, a solution of 10  $\mu\text{g ml}^{-1}$  rhodamine-conjugated fibronectin (Cytoskeleton, Inc.) in 30 mM  $\text{CaCl}_2$  was used for the coating. After the 30 min coating at room temperature, the film was rinsed with a phosphate-buffered saline (PBS) solution. Then, a  $3 \times 10^5$  cells per ml cell

suspension of HUVECs was applied to the film and incubated for 1 h to enable cell attachment to the film surface. A solution of 1  $\text{mg ml}^{-1}$  alginate lyase (Sigma-Aldrich) was added to dissolve the sacrificial Ca-alginate layer. The medium was exchanged with a fresh one three times to remove the remaining alginate lyase. This enzymatic release of the film induces self-folding in a few seconds without cytotoxicity.<sup>11,26</sup> For co-culturing HUASMCs with HUVECs, a  $1 \times 10^5$  cells per ml cell suspension of HUASMCs was added 12 h after encapsulating HUVECs. All cultures were maintained in a  $\text{CO}_2$  incubator (5%; 37  $^\circ\text{C}$ ; humidified air).

### Immunocytochemistry

Immunocytochemistry was performed as described previously.<sup>15</sup> The culture was fixed with a solution of 4% paraformaldehyde

(Sigma-Aldrich) in PBS for 30 min at room temperature. After three cycles of rinsing with PBS, the culture was treated with a solution of 0.01 wt% TritonX 100 (Sigma-Aldrich) and 0.1 wt% bovine serum albumin (Sigma-Aldrich) in PBS for 3 h at 4 °C to enhance the permeability of the cell membrane and block non-specific antibody binding. The following primary antibodies were used: anti-CD31 (1 : 500 dilutions, Abcam), anti-ZO1 (1 : 500 dilutions, Abcam), anti-podocalyxin (PODXL; 1 : 500 dilutions, Abcam), and anti- $\alpha$ -smooth muscle actin ( $\alpha$ -SMA; 1 : 500 dilutions, Abcam). Additionally, Acti-stain™ 488 phalloidin (1 : 500 dilution, cytoskeleton) was used to stain actin. To visualize nuclei, a solution of 10  $\mu\text{g ml}^{-1}$  Hoechst 33342 was added to the culture. The images were obtained using confocal fluorescence microscopy (FLUOVIEW FV3000; Olympus).

### Calcium imaging

To characterize the responses in HUASMCs upon pharmacological stimulation, their intracellular  $\text{Ca}^{2+}$  concentration was monitored using a fluorescent calcium binding dye (Fluo-8; Abcam). The culture of HUASMCs was loaded with a solution of 4- $\mu\text{M}$  Fluo-8 AM and 0.02 wt% pluronic F127 at 37 °C for 30 min. The cultures were observed using a confocal fluorescence microscope (SD-OSR; Olympus) with a stage-top incubator (Tokai Hit) in 5%  $\text{CO}_2$  at 37 °C with humidified air. The images were obtained at ten frames per second.

### Scanning electron microscopy

The detailed structure of the cell-laden film was observed using a scanning electron microscopy system (Auriga 60 Cross Beam Workstation, Carl Zeiss). The culture was fixed with a solution of 2 wt% glutaraldehyde (FUJIFILM Wako Chemicals) for 2 h and then dehydrated with ethanol, followed by immersion in *tert*-butyl alcohol (FUJIFILM Wako Chemicals). Then, the culture was lyophilized using a freeze dryer (FS-2030, EYELA) and coated with Au (10 nm) using an ion sputter gun (E-1030, Hitachi).

## Results and discussion

### Vascular endothelial cell culture within the self-folded film

To prove the concept of tubular-tissue formation inside the folded film, we examined how encapsulated HUVECs formed a three-dimensional culture through microscopic observation. As shown in Fig. 1A and B, HUVECs were encapsulated in porous self-folding films and cultured. The enhanced diffusion of oxygen and nutrients through the pores enabled the cell culture to form within the confined structure, resulting in the growth and migration of HUVECs on the inner wall of the micro-roll (Movie S1, ESI†). Live/dead staining images are shown in Fig. S3 (ESI†). Since the cell density was high inside the micro-roll, several HUVECs migrated from the inside to the outside of the micro-roll on the first day of culturing. The remaining HUVECs took elongated cell morphologies and formed a confluent culture on the inner surface of the micro-roll after two days of culturing. Note that the cell viability was not significantly

decreased. The growth of HUVECs results in the formation of tubular tissue along the wall of the micro-roll (Fig. 1C–E). The tubular tissue was formed in batches because an array of self-folding films was fabricated. Importantly, their ability to form a confluent monolayer resulted in the hollow structure. As described in previous studies, other types of cells such as neurons, cardiomyocytes, and skeletal muscle cells have been demonstrated to occupy the inner space of the micro-roll and form cylindrical tissue.<sup>15</sup> In contrast, the scanning electron microscopy (SEM) images in Fig. 1E show the formation of a thin HUVEC monolayer on the inner film surface. Furthermore, immunocytochemical images in Fig. 1F and G show the expression of proteins characteristic of the endothelium. PODXL was highly expressed at the apical membrane of HUVECs, indicating apical-basal polarization of HUVECs (Fig. 1F). ZO1, a tight junction protein, was expressed at the cell boundary in the monolayer of confluent HUVECs, suggesting an endothelial barrier function. Thus, these results indicate that the self-folded film works as a cell scaffold for the formation of vascular endothelial tissue.

The curvature of tubular tissue can be controlled because that of the micro-roll is tuneable (Fig. 2). As described in previous work, the internal strain gradient between the atom-thick graphene and nanometre-thick parylene-C induces self-folding, forming the ten-micron-scale micro-roll.<sup>15,24,25</sup> The curvature of the micro-roll depends on the film thickness, which can be controlled by the amount of dichloro-di(*p*-xylylene) laden in the parylene-C CVD process. Since HUVECs form a thin monolayer along the inner wall of the micro-roll, the size of the tubular tissue might depend on the thickness of the parylene-C layer. The cross-sectional view of the tubular tissue demonstrates that the curvature radius of the tubular tissue decreased as the thickness of the parylene-C layer increased (Fig. 2A). For the parylene-C thickness of  $t_p = 90$  nm, the folded film formed twin rolls like a dumbbell because the minimum width of the film was 300  $\mu\text{m}$ , while the curvature radius was  $12.5 \pm 0.8$   $\mu\text{m}$ . Despite the narrow structure, the hollow structure was maintained because HUVECs form a cell monolayer. Although previous work utilized the cell contraction force to drive the self-folding of the film,<sup>27</sup> the curvature radius of the micro-rolls was not significantly affected by the culture of HUVECs, probably because the contraction force of HUVECs is weaker than that of other cell types (Fig. S5, ESI†). Thus, the curvature of the tubular tissue can be controlled by adjusting the thickness of the parylene-C layer (Fig. 2B). The range of the curvature radius is comparable to that of the typical human arteriole (15–300  $\mu\text{m}$ ).<sup>1,23</sup> Importantly, it is technically challenging to create a cellular construct with a micron-scale diameter using other fabrication methods such as microfluidics, moulding, and bioprinting.<sup>3,6</sup> Additionally, the typical size of a self-organized capillary network is 1–3  $\mu\text{m}$ . While a 50  $\mu\text{m}$ -diameter cellular construct was previously created by encapsulating vascular cells within a self-folding film, we verify that this cell encapsulation approach is applicable to the formation of tubular tissue smaller than 50  $\mu\text{m}$ . The tunability of the micron-scale curvature enables

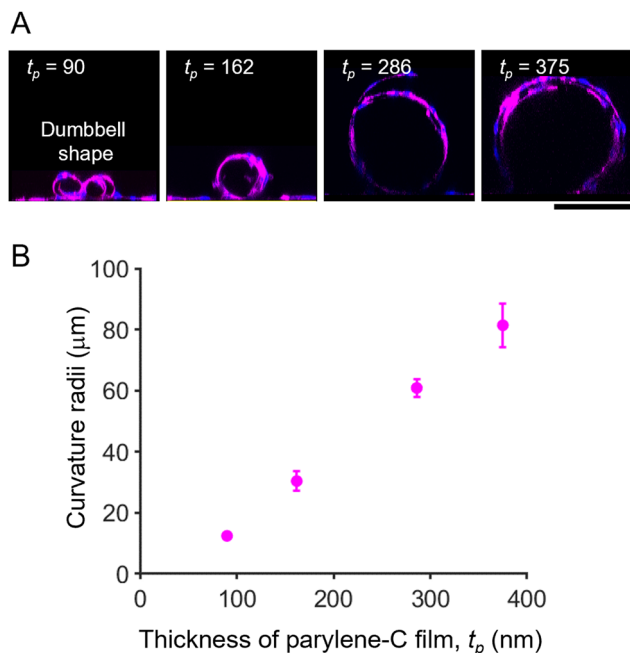


**Fig. 2** Diameter control of tubular HUVEC culture by adjusting the parylene-C thickness. (A) Representative cross-sectional images of HUVECs encapsulated in micro-rolls with varying parylene-C thickness. HUVECs were visualized by immunocytochemistry using anti-CD31 antibody (magenta) and Hoechst 33342 (blue). (B) Plots of curvature radii versus parylene-C film thickness. The curvature increased with the thickening of the parylene-C layer. Note that the parylene-C thickness can be adjusted by varying the amount of parylene-C dimer in the CVD process. Scale bars indicate 100  $\mu\text{m}$ . The error bars represent the standard deviations of the mean.  $n > 15$  micro-rolls.

us to mimic the tubular structure of a small artery. The tubular structure is also useful for applying this model to fluidics applications with haemocytes. Since parylene-C is blood compatible and has low thrombogenicity,<sup>28,29</sup> introducing a blood flow inside the micro-roll enables us to investigate how haemocytes interact with endothelial cells. Further experiments culturing haemocytes will help us construct a more complex model of a small artery.

### Smooth muscle cell culture on the outer surface of the micro-roll

We then cultured HUASMCs to confirm that they can grow on the outer surface of the micro-roll. The film was self-folded prior to cell seeding, and then HUASMCs were seeded onto the micro-roll (Fig. 3A). Immunocytochemical images in Fig. 3B show the growth of HUASMCs on the surface of the micro-roll. To visualize the micro-roll, rhodamine-conjugated fibronectin was coated on the surface of the film, which became the inner surface of the micro-roll. Although the outer surface of the micro-roll was not treated by proteins, HUASMCs were grown on the surface due to the high cytocompatibility of graphene. As shown in Fig. 3B, they formed actin stress fibres (cyan) along with the expression of  $\alpha$ -SMA (green), a smooth muscle-specific actin isoform. In addition, the HUASMCs exhibited calcium responses to the 0.5  $\mu\text{M}$  ET-1 application (Fig. 3C). Endothelial

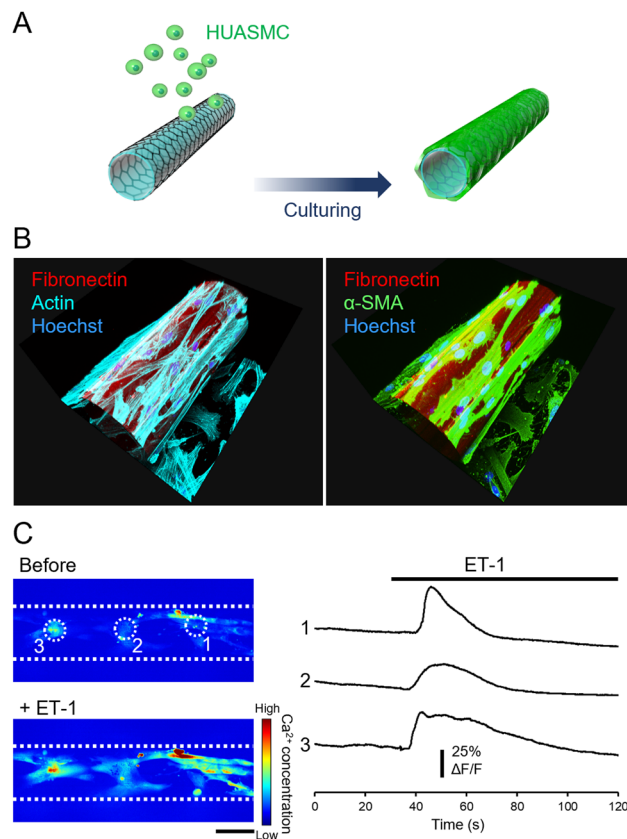


**Fig. 3** Culture of HUASMCs on the outer surface of a micro-roll. (A) The process of culturing HUASMCs: they were seeded onto the micro-roll after self-folding the film. (B) 3D reconstructions of immunocytochemical images of HUASMCs. Rhodamine-conjugated fibronectin, coated on the surface of the self-folding film, visualized the micro-roll. (C) Images and intensity profiles of intracellular calcium concentration in HUASMCs before and after the application of 0.5  $\mu\text{M}$  ET-1, an endothelium-derived vasoactive substance. The intensity profile was obtained from different cells indicated by white dotted circles in the images. White dotted lines indicate the wall of the micro-roll.

ET-1 is known to induce smooth muscle contraction *via*  $\text{Ca}^{2+}$  influx.<sup>30,31</sup> The HUASMCs also responded to the 100  $\mu\text{M}$  phenylephrine, the  $\alpha$ -1 adrenergic receptor agonist (Fig. S6, ESI†). The  $\alpha$ -1 adrenergic receptors mediate smooth muscle contraction through sympathetic nerve activation.<sup>30,31</sup> Thus, the HUASMCs were matured on the surface of the micro-roll and maintained their responsiveness to vasoactive substances.

### Vascular endothelial cells/smooth muscle cells co-cultured across the porous wall of the micro-roll

Since the HUVECs and HUASMCs were successfully cultured on the wall of a micro-roll, we separately co-cultured them across the wall of the micro-roll to demonstrate that the cell-laden micro-roll mimics the laminar structure of an artery, including the endothelium, IEL, and smooth muscle (Fig. 4A and B). As shown in Movie S2, ESI†, HUVECs and HUASMCs grew inside and outside the micro-roll, respectively. On day 2 of culture, the formation of laminar tissues along the wall of the micro-roll was observed by confocal microscopy (Fig. 4C). In particular,

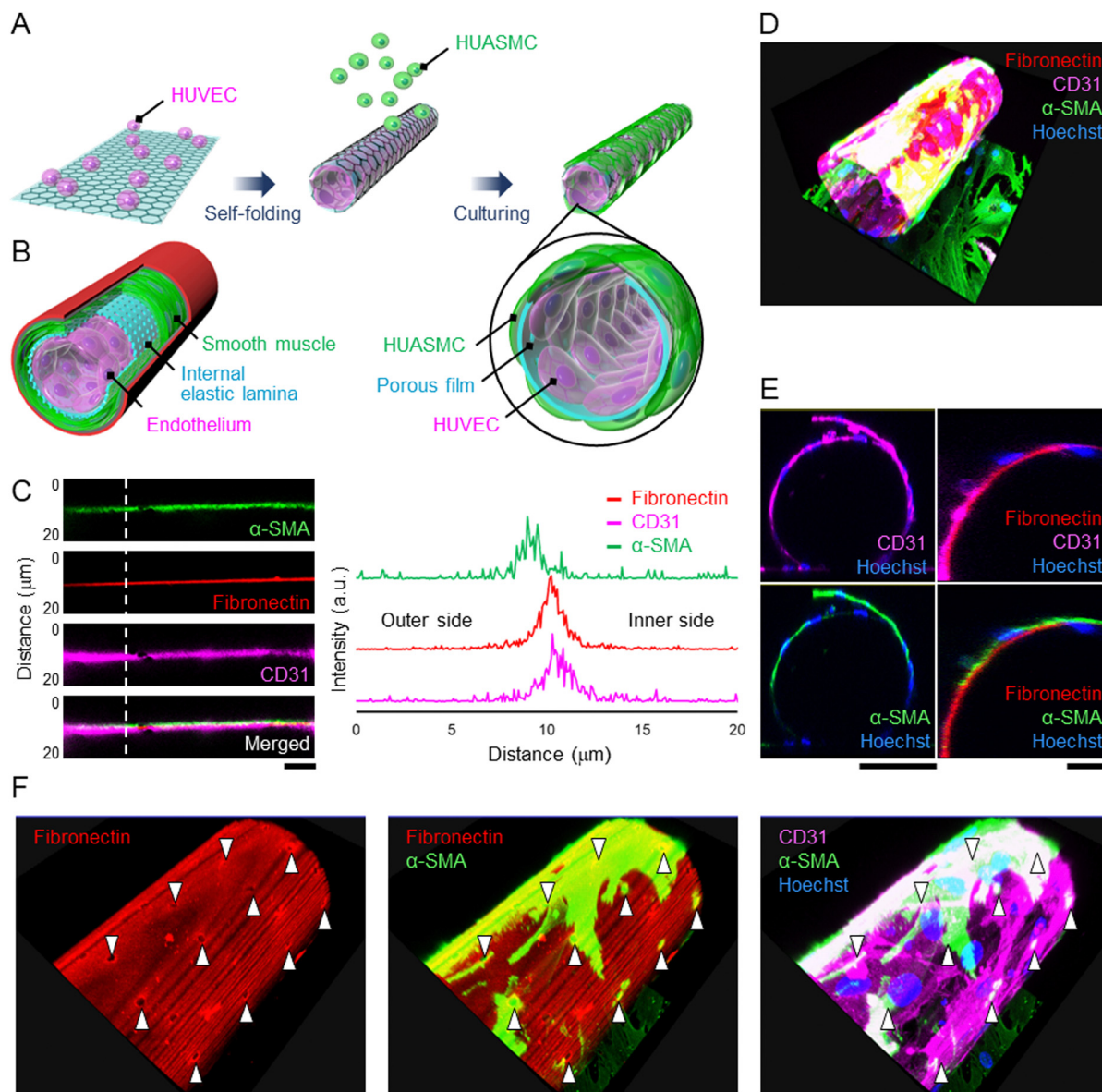


**Fig. 4** Co-culture of HUVECs and HUASMCs separately on the inner and outer surfaces of the micro-roll. (A) The process of co-culturing HUVECs and HUASMCs: HUVECs were encapsulated within the micro-roll, and HUASMCs were then seeded onto the cell-laden micro-roll. (B) Schematic image of the artery wall. The porous film acts as a barrier while enabling intercellular communication between the two cell layers, similar to the structural function of the internal elastic lamina (IEL). (C) Magnified immunocytochemical images of the wall of the micro-roll and the intensity profile along the white dotted line. HUVECs and HUASMCs were visualized using anti-CD31 (magenta) and anti- $\alpha$ -SMA (green) antibodies, respectively. Note that the inner surface was coated with rhodamine-conjugated fibronectin (red) to indicate the boundary between the outer and inner sides of the micro-roll. In these images, the upper side represents the outer side of the micro-roll. (D) 3D reconstruction of immunocytochemical images of co-cultured HUVECs and HUASMCs. (E) Cross-sectional view of the cell-laden micro-roll, indicating the formation of a tubular structure. (F) 3D reconstructed images showing  $\alpha$ -SMA-positive HUASMCs on the porous surface. White arrowheads indicate the pores on the wall of the micro-roll. Note that  $\alpha$ -SMA was highly expressed at the pores. Scale bars indicate 10  $\mu$ m (C) and 100  $\mu$ m (E).

the intensity profile at the vertical line of the wall enables us to examine the location of both HUVEC and HUASMC layers relative to the fibronectin-coated wall. The intensity peak of CD31 was on the inner side of the micro-roll, while the peak of  $\alpha$ -SMA was exhibited on the outer side. The intensity peak of CD31 was closer to that of fibronectin than that of  $\alpha$ -SMA because fibronectin was coated on the inner surface. These peak positions indicate that the layers of HUVECs and

HUASMCs were formed on the inner and outer surfaces of the wall, respectively. Then, the co-cultured cells adhered to the different surfaces, resulting in the formation of layered tubular tissue that mimics the physiological assembly of an artery (Fig. 4D and E). Although the wall separated the cell layers, the pores enabled intercellular communication between HUVECs and HUASMCs. As shown in Fig. 4F,  $\alpha$ -SMA in HUASMCs was highly expressed at the pores. Cell-cell

interactions *via* direct contact and paracrine between HUVECs and HUASMCs potentially promoted the formation of actin fibres in HUASMCs. This result suggests that the porous wall of the micro-roll works as a permeable barrier, modulating the intercellular interactions between endothelial cells and smooth muscle cells, which is similar to the structural function of IEL.

The tunability of 3D geometries, including the curvature, pore size, and pore density, is one of the main advantages of self-folding devices. Both graphene and parylene-C film can be etched using reactive ion etching with photolithography, enabling easy acquisition of a 2D micro-pattern on the self-folding film. Furthermore, by taking advantage of the transferable property of a two-dimensional micro-pattern onto a 3D curved surface, the pore pattern can be designed on the wall of the micro-roll. The size and density of pores on the IEL are key parameters in vascular development and diseases because they affect intercellular communications *via* diffusible substances, myoendothelial junctions, and the migration of smooth muscle cells into the endothelium.<sup>17–19</sup> As previously reported, the pore size on this self-folding film can be adjusted from 2 to 13  $\mu\text{m}$  on this self-folding film.<sup>15</sup> The range is comparable to the pores in the IEL (0.5–10  $\mu\text{m}$ ).<sup>17,32</sup> Additionally, the wide range of the micro-roll's pore density from 1.8 to 75% is applicable to the mimicry of the pore density in the IEL ranging from 2 to 20%.<sup>15,17</sup> Furthermore, although the typical thickness of the IEL is 1–3  $\mu\text{m}$ ,<sup>33</sup> the depth of the myoendothelial cell-cell contact was reported to be 100 nm,<sup>17</sup> which corresponds to the thickness of the micro-roll's wall, suggesting that the film's pore facilitates the myoendothelial junctions. Thus, the tunability and scalability of 3D geometries, including thickness, curvature, and porosity, enable us to emulate the microenvironmental geometries of the IEL in both physiological and pathological conditions. Further studies investigating myoendothelial junctions, secretion of vasoactive substances, and migration of smooth muscle cells will reveal how the 3D geometries affect the cellular functions.

## Conclusion

We have demonstrated a small-artery-mimicking co-culture model using a self-folding graphene-based porous micro-roll. Taking advantage of the tunability of the curvature radius of the micro-roll, cell encapsulation of HUVECs within the micro-roll created a cellular construct that has a tubular structure smaller than 50  $\mu\text{m}$ . Furthermore, HUASMCs were successfully cultured on the outer surface of the micro-roll. Consequently, HUVECs and HUASMCs were separately co-cultured on the inner and outer surfaces of the micro-roll, respectively. The porous wall of the micro-roll acts as a boundary between HUVECs and HUASMCs while enabling cell-cell communications *via* pores, which is similar to the IEL in the artery wall. Thus, the cellular construct recapitulated key characteristics of a small artery, including the precise geometries, cellular compositions, ECM structure, and layered tubular structure. The co-culture system would be utilized to investigate intercellular communications

while maintaining the artery-like structure and help us better understand the mechanisms of vascular development and disease in the small artery.

## Author contributions

Conceptualization: K. S., S. M., and T. T. Data curation: K. S. Formal analysis: K. S. Funding acquisition: M. Y. Investigation: K. S., S. M., T. T., and T. G. Methodology: K. S., S. M., and T. T. Project administration: S. T. and M. Y. Resources: S. T. and M. Y. Software: K. S. Supervision: S. T. and M. Y. Validation: K. S., S. M., T. T., and T. G. Visualization: K. S., S. M., and T. G. Writing – original draft: K. S. Writing – review & editing: S. M., T. T., T. G., S. T., and M. Y.

## Conflicts of interest

There are no conflicts to declare.

## Acknowledgements

We thank Y. Furukawa for assistance regarding cell culture.

## References

- 1 F. Feihl, L. Liaudet, B. Waeber and B. I. Levy, *Hypertension*, 2006, **48**, 1012–1017.
- 2 W. Herrington, B. Lacey, P. Sherliker, J. Armitage and S. Lewington, *Circ. Res.*, 2016, **118**, 535–546.
- 3 K. Gold, A. K. Gaharwar and A. Jain, *Biomaterials*, 2019, **196**, 2–17.
- 4 J. Chen, X. Zhang, R. Millican, T. Lynd, M. Gangasani, S. Malhotra, J. Sherwood, P. T. Hwang, Y. Cho, B. C. Brott, G. Qin, H. Jo, Y. S. Yoon and H. W. Jun, *Front. Cardiovasc. Med.*, 2021, **8**, 790529.
- 5 S. Alimperti, T. Mirabella, V. Bajaj, W. Polacheck, D. M. Pirone, J. Duffield, J. Eyckmans, R. K. Assoian and C. S. Chen, *Proc. Natl. Acad. Sci. U. S. A.*, 2017, **114**, 8758–8763.
- 6 A. J. Boys, S. L. Barron, D. Tilev and R. M. Owens, *Front. Bioeng. Biotechnol.*, 2020, **8**, 589960.
- 7 A. Hasan, A. Paul, N. E. Vrana, X. Zhao, A. Memic, Y. S. Hwang, M. R. Dokmeci and A. Khademhosseini, *Biomaterials*, 2014, **35**, 7308–7325.
- 8 A. Shimizu, W. H. Goh, S. Itai, M. Hashimoto, S. Miura and H. Onoe, *Lab Chip*, 2020, **20**, 1917–1927.
- 9 Y. Mei, G. Huang, A. A. Solovev, E. B. Ureña, I. Mönch, F. Ding, T. Reindl, R. K. Fu, P. K. Chu and O. G. Schmidt, *Adv. Mater.*, 2008, **20**, 4085–4090.
- 10 M. Jamal, S. S. Kadam, R. Xiao, F. Jivan, T. M. Onn, R. Fernandes, T. D. Nguyen and D. H. Gracias, *Adv. Healthcare Mater.*, 2013, **2**, 1142–1150.
- 11 T. F. Teshima, H. Nakashima, Y. Ueno, S. Sasaki, C. S. Henderson and S. Tsukada, *Sci. Rep.*, 2017, **7**, 17376.
- 12 S. Cheng, Y. Jin, N. Wang, F. Cao, W. Zhang, W. Bai, W. Zheng and X. Jiang, *Adv. Mater.*, 2017, **29**, 1700171.

- 13 R. Arayanarakool, A. K. Meyer, L. Helbig, S. Sanchez and O. G. Schmidt, *Lab Chip*, 2015, **15**, 2981–2989.
- 14 Q. Jin, A. Bhatta, J. V. Pagaduan, X. Chen, H. West-Foyle, J. Liu, A. Hou, D. Berkowitz, S. C. Kuo, F. B. Askin, T. D. Nguyen, D. H. Gracias and L. H. Romer, *Sci. Adv.*, 2020, **6**, eaaz2598.
- 15 K. Sakai, T. F. Teshima, H. Nakashima and Y. Ueno, *Nanoscale*, 2019, **11**, 13249–13259.
- 16 K. Sakai, T. F. Teshima, T. Goto, H. Nakashima and M. Yamaguchi, *Adv. Funct. Mater.*, 2023, **33**, 2301836.
- 17 S. L. Sandow, D. J. Gzik and R. M. Lee, *J. Anat.*, 2009, **214**, 258–266.
- 18 J. Ledoux, M. S. Taylor, A. D. Bonev, R. M. Hannah, V. Solodushko, B. Shui, Y. Tallini, M. I. Kotlikoff and M. T. Nelson, *Proc. Natl. Acad. Sci. U. S. A.*, 2008, **105**, 9627–9632.
- 19 Y. W. Lu, A. M. Lowery, L. Y. Sun, H. A. Singer, G. Dai, A. P. Adam, P. A. Vincent and J. J. Schwarz, *Arterioscler., Thromb., Vasc. Biol.*, 2017, **37**, 1380–1390.
- 20 K. Hatherell, P. O. Couraud, I. A. Romero, B. Weksler and G. J. Pilkington, *J. Neurosci. Methods*, 2011, **199**, 223–229.
- 21 N. C. A. van Engeland, A. Pollet, J. M. J. den Toonder, C. V. C. Bouten, O. Stassen and C. M. Sahlgren, *Lab Chip*, 2018, **18**, 1607–1620.
- 22 S. Miura, K. Sato, M. Kato-Negishi, T. Teshima and S. Takeuchi, *Nat. Commun.*, 2015, **6**, 8871.
- 23 D. Short, *Br. Heart J.*, 1966, **28**, 184–192.
- 24 T. F. Teshima, C. S. Henderson, M. Takamura, Y. Ogawa, S. Wang, Y. Kashimura, S. Sasaki, T. Goto, H. Nakashima and Y. Ueno, *Nano Lett.*, 2019, **19**, 461–470.
- 25 T. Goto, T. F. Teshima, K. Sakai and M. Yamaguchi, *AIP Adv.*, 2022, **12**, 075002.
- 26 T. Teshima, H. Onoe, K. Kuribayashi-Shigetomi, H. Aonuma, K. Kamiya, H. Ishihara, H. Kanuka and S. Takeuchi, *Small*, 2014, **10**, 912–921.
- 27 K. Kuribayashi-Shigetomi, H. Onoe and S. Takeuchi, *PLoS One*, 2012, **7**, e51085.
- 28 M. Golda-Cepa, K. Engvall, M. Hakkarainen and A. Kotarba, *Prog. Org. Coat.*, 2020, **140**, 105493.
- 29 B. A. Weisenberg and D. L. Mooradian, *J. Biomed. Mater. Res.*, 2002, **60**, 283–291.
- 30 F. V. Brozovich, C. J. Nicholson, C. V. Degen, Y. Z. Gao, M. Aggarwal and K. G. Morgan, *Pharmacol. Rev.*, 2016, **68**, 476–532.
- 31 M. J. Berridge, *J. Physiol.*, 2008, **586**, 5047–5061.
- 32 H. Masuda, Y. J. Zhuang, T. M. Singh, K. Kawamura, M. Murakami, C. K. Zarins and S. Glagov, *Arterioscler., Thromb., Vasc. Biol.*, 1999, **19**, 2298–2307.
- 33 V. D. Aiello, P. S. Gutierrez, M. J. Chaves, A. A. Lopes, M. L. Higuchi and J. A. Ramires, *Mod. Pathol.*, 2003, **16**, 411–416.